JGR Biogeosciences

RESEARCH ARTICLE
10.1029/2018JG004917

No Proportional Increase of Terrestrial Gross Carbon Sequestration From the Greening Earth

Yulong Zhang[1,2], **Conghe Song**[1,2], **Lawrence E. Band**[3,4], **and Ge Sun**[5]

[1]Department of Geography, University of North Carolina at Chapel Hill, Chapel Hill, NC, USA, [2]Institute for the Environment, University of North Carolina at Chapel Hill, Chapel Hill, NC, USA, [3]Department of Environmental Science, University of Virginia, Charlottesville, VA, USA, [4]Department of Civil and Environmental Engineering, University of Virginia, Charlottesville, VA, USA, [5]Eastern Forest Environmental Threat Assessment Center, Southern Research Station, USDA, Forest Service, Raleigh, NC, USA

Key Points:
- Global terrestrial GPP did not increase in proportion to the greening on Earth
- Enhanced global terrestrial GPP largely contributed by nonforests, especially cropland
- Contrasting GPP changes in forest and cropland may have shifted the distribution of land carbon sink

Supporting Information:
- Supporting Information S1

Correspondence to:
Y. Zhang and C. Song,
ylzhang@unc.edu;
csong@email.unc.edu

Citation:
Zhang, Y., Song, C., Band, L. E., & Sun, G. (2019). No proportional increase of terrestrial gross carbon sequestration from the greening Earth. *Journal of Geophysical Research: Biogeosciences*, *124*, 2540–2553. https://doi.org/10.1029/2018JG004917

Received 6 NOV 2018
Accepted 23 JUL 2019
Accepted article online 5 AUG 2019
Published online 17 AUG 2019

Author Contributions:
Conceptualization: Yulong Zhang, Conghe Song, Lawrence E. Band, Ge Sun
Data curation: Yulong Zhang
Formal analysis: Yulong Zhang
Investigation: Yulong Zhang
Methodology: Yulong Zhang
Resources: Yulong Zhang
Software: Yulong Zhang
Validation: Yulong Zhang
Visualization: Yulong Zhang
Writing - original draft: Yulong Zhang
Writing – review & editing: Yulong Zhang, Conghe Song, Lawrence E. Band, Ge Sun

Abstract Terrestrial vegetation, as the key component of the biosphere, has a greening trend since the beginning of this century. However, how this substantial greening translated to global gross carbon sequestration or gross primary production (GPP) is not clear. Here we investigated terrestrial GPP dynamics and the respective contributions of climate change and vegetation cover change (VCC) from 2000 to 2015. We adopted a remote sensing based data-driven model, which was calibrated based on the global eddy flux data set (FLUXNET2015) and Moderate Resolution Imaging Spectroradiometer vegetation index data (Collection 6). A series of simulation experiments were conducted to disaggregate the effects of climate and VCC. We found a much weaker increase in global GPP (0.08%/year; $P = 0.07$) when compared with the global greening rate (0.23%/year; $P < 0.001$). The positive effect of VCC on GPP was reduced by 53% due to climate stress. Enhanced global GPP were largely contributed by nonforests, especially croplands. However, tropical forests, once a major driver of the global GPP increase, negatively contributed to global GPP trend due to warming-induced moisture stress and deforestation. Given the limited potential of cropland carbon storage due to harvest and consumption, the contrasting GPP changes (i.e., cropland GPP increase vs. forest GPP reduction) may have shifted the distribution of the land carbon sink. Our study highlights the potential vulnerability of terrestrial gross carbon sequestration under climate and land use changes and has important implications in the global carbon cycle and climate warming mitigation.

1. Introduction

As the key component of the biosphere, terrestrial vegetation absorbs atmospheric CO_2 through photosynthesis and serves as a major mechanism to potentially offset anthropogenic CO_2 emissions, thus contributing to climate mitigation and human welfare (Lieth & Whittaker, 2012; Running, 2012). The amount of total carbon captured by plants via photosynthesis in a unit time is defined as gross primary production (GPP). As the largest CO_2 flux from the atmosphere to the biosphere, terrestrial GPP primarily drives the global carbon cycle (Houghton, 2007) and provides the essential matter and energy basis for ecosystem functions such as respiration and growth (Beer et al., 2010). However, terrestrial GPP is one of the most variable components in the carbon cycle (Anav et al., 2013; Lieth & Whittaker, 2012; Running et al., 2004), and its dynamics and responses to the changing environment remain poorly understood (Anav et al., 2015; Campbell et al., 2017).

Earth observations from space have shown a widespread greening over the land surface since the beginning of this century (Chen et al., 2019; Zhang, Song, et al., 2017; Zhu et al., 2016). However, how this substantial greening translates to gross carbon sequestration or GPP, especially in the context of climate change, is not well established. The greening could lead to a proportional increase in GPP by enhancing the absorbed photosynthetic active radiation (Potter et al., 1993). Climate warming may further alleviate temperature stress in cold regions, increasing GPP (Nemani et al., 2003). However, high temperature and low precipitation following the ongoing warming may increase climate stress, reducing GPP (Anderegg et al., 2015; Ciais et al., 2005; Zhao & Running, 2010). Global GPP dynamics are further complicated by human-induced land use change such as deforestation (Cramer et al., 2004; Malhi et al., 2008). To date, a consensus on global GPP dynamics and the driving forces are still elusive (Anav et al., 2015; Campbell et al., 2017; Jung et al., 2017; Ryu et al., 2019; Welp et al., 2011; Zhao & Running, 2010).

Ecosystem models in combination with remotely sensed observations provide an unprecedented way to explore global GPP dynamics (Anav et al., 2015; Beer et al., 2010). However, the model performance largely depends on the quality of remote sensing data, especially on the long-term scales (Hilker et al., 2008). The Advanced Very High Resolution Radiometer (AVHRR) sensors onboard the National Oceanic and Atmospheric Administration satellite series provide the longest continuous spectral measurements on the land surface since 1981 (Pettorelli et al., 2005). The AVHRR-based products such as normalized difference vegetation index (NDVI) and leaf area index (LAI) have been key vegetation data in global change studies (Pinzon & Tucker, 2014; Zhu et al., 2013). However, recent studies showed that large inconsistences exist in these long-term products mainly due to sensor differences and platform drift (Jiang et al., 2017; Tian et al., 2015). The Moderate Resolution Imaging Spectroradiometer (MODIS) onboard National Aeronautics and Space Administration's Terra and Aqua satellites since 2000 are referred to as the extension of AVHRR-based observations with advanced spectral, spatial, and temporal characteristics (Song et al., 2015). However, recent studies indicated that MODIS Collection 5 data, which were widely used to understand vegetation dynamics, suffered from sensor degradation, especially for Terra satellite after 2009 (Lyapustin et al., 2014; Wang et al., 2012; Zhang, Song, et al., 2017). Consequently, these data uncertainties may have been propagated into the related global GPP studies.

Here, we aim to investigate terrestrial GPP dynamics and quantify the respective contributions of climate change and vegetation cover change (VCC) from 2000 to 2015 using a newly developed coupled carbon and water (CCW) model (Zhang et al., 2016). The CCW model was calibrated based on the global eddy flux data set from FLUXNET2015 and MODIS Collection 6 (C6) NDVI data. Compared to C5, MODIS-C6 NDVI has implemented several improvements in the retrieval algorithm (Didan et al., 2015) and corrected the major sensor degradation impacts identified by previous studies (Lyapustin et al., 2014; Zhang, Song, et al., 2017). To better account for VCC effect on GPP, we adopted the yearly land cover product from the European Space Agency Climate Change Initiative (ESA-CCI). Model evaluations for CCW were conducted based on the flux tower data, FLUXCOM GPP, MODIS GPP products, and solar-induced fluorescence (SIF) data from the Orbiting Carbon Observatory-2 (OCO-2). A series of experiments were designed to disaggregate the effects of climate and VCC on global GPP, aiming to understand how recent greening translated into gross carbon sequestration. Our hypothesis is that the terrestrial GPP increases proportionally as the Earth greens up.

2. Materials and Methods

2.1. Global Data Set

Global satellite products used in this study included global monthly vegetation index data from MODIS (data version: MOD13C2 C6; spatial resolution: 0.05°; period: 2000–2015), annual land cover data from ESA-CCI (300 m; 2000–2015), annual MODIS GPP product (V55; 1 km; 2000–2015), annual FLUXCOM GPP product (0.5°; 1982–2013), and monthly SIF data from OCO-2 (1°; 2015). Global monthly climate data were from CRU-National Centers for Environmental Prediction (NCEP; V7; 0.5°; 2000–2015). Global monthly covariance eddy flux data were from FLUXNET2015 (updated on 3 November 2016; 2000–2014). Other data included Köppen-Geiger climate classification (0.5°) and global forest area from Food and Agriculture Organization (FAO) Forestry inventory (2000, 2005, 2010, 2015). The data sources used in this study were described in Text S1 in the supporting information.

2.2. Model Framework

We developed the CCW model to estimate terrestrial ecosystem GPP and evapotranspiration simultaneously at a monthly scale using global eddy flux tower data from FLUXNET and remotely sensed data from MODIS (Zhang et al., 2016). Based on the light-use efficiency (LUE) theory (Potter et al., 1993), GPP in CCW is estimated as the product of absorbed photosynthetically active radiation and realized LUE (ε) that varies with vegetation types and climate:

$$GPP = APAR \times \mathscr{E} = (PAR \times FPAR) \times \left(\mathscr{E}_{\text{pot}} \times R_s \times T_s \times W_s\right) \quad (1)$$

where PAR is the incident photosynthetically active radiation (MJ/m^2), which is assumed to be 45% of the shortwave total radiation (Running et al., 2000); $FPAR$ is the fraction of PAR absorbed by plants, which is

linear to NDVI (Sims et al., 2006) ; ε_{pot} (g C/MJ) is the potential LUE realized by plants without environmental stresses; R_s, T_s, and W_s are the environmental scalars related to diffuse radiation proportion, air temperature, and vapor pressure deficit (VPD), each of which varies within the range of 0–1. The model is capable of estimating large-scale GPP with acceptable accuracy. Compared to other models (e.g., MOD17), CCW model considers the nonlinear constrains of temperature and VPD and the effect of light saturation on LUE. The details of the theory framework identification for CCW can be found in Zhang et al. (2016).

2.3. Model Calibration and Validation

The initial version of CCW was calibrated based on LaThuile 2007 FLUXNET Synthesis Dataset and Terra MODIS-C5 NDVI. Given that global eddy flux tower data and MODIS NDVI data have been updated to FLUXNET2015 and MODIS-C6 NDVI data, respectively, we recalibrated CCW based on those up-to-date data. Notably, the FLUXNET2015 data set has expanded its data records from 2006 to 2014 and includes several improvements in the data quality control protocols and the data processing pipeline compared to its predecessor LaThuile 2007 data set (www.fluxnet.fluxdata.org/data/). Our evaluation showed that MODIS-C6 NDVI from Terra satellite is more consistent with vegetation index products from the Aqua satellite and sensor degradation impact has been largely removed (Zhang, Song, et al., 2017).

The site-level data used to calibrate CCW are from FLUXNET2015 and 1-km MODIS-C6 NDVI during 2000 to 2014. After data screening (Zhang et al., 2016), a total of 8,309 monthly records covering 9 biomes at 155 flux tower sites was selected (Table S1). Spatially, these sites span a wide range of climate zones from the boreal/alpine and temperate to arid/semiarid and tropics (Figure 1). We randomly split data records at each flux site and then used half of the data within each biome to recalibrate all biome-specific parameters in CCW through Monte Carlo simulation (Zhang et al., 2016). The recalibrated parameters are seen in Table S2. The reserved data were used to evaluate the model at whole, biome, and site levels.

2.4. Estimation and Evaluation of Global GPP by CCW

The global data set used to drive CCW in this study include 0.5° × 0.5° monthly climate data from CRU-NCEP V7 (2000–2015), 0.05° × 0.05° monthly NDVI data from Terra-MODIS product (i.e., MOD13C2 C6), and 300 × 300-m annual land cover data from ESA-CCI.

The CRU-NCEP climate data are the combination of ground observation-based CRU and model-based NCEP-National Center for Atmospheric Research Reanalysis data (Viovy, 2018). We downloaded 6-hourly CRU-NCEP data sets including global radiation, precipitation, air temperature, air pressure, and air specific humidity. VPD was calculated using air temperature, atmospheric pressure, and air specific humidity at the 6-hourly scale and then aggregated into the monthly scale. The coarse spatial data were downscaled to the spatial resolution of 5 × 5 km^2 with bilinear interpolation.

Land cover data were used to define the maximum LUE and climate constrains for each plant functional type in CCW. In this study, we adopted the annual global land cover product from the CCI of the ESA. This product is a consistent global land cover data at 300-m spatial resolution on an annual basis from 1992 to 2015. The original ESA-CCI data uses the Land Cover Classification System developed by the United Nations FAO (Table S3). To serve CCW, we converted the United Nations-Land Cover Classification System in ESA-CCI product to the classification of International Geosphere-Biosphere Programme based on the conversion (Table S4) and then aggregated the 300 × 300-m data to the spatial resolution of 5 × 5 km^2 by computing biome compositions. With input data described above, we then estimated global GPP by weighting biome area proportions within each 5 × 5-km^2 pixel.

To evaluate global GPP estimated by CCW, we collected the machine learning (ML)-based GPP product from FLUXCOM (three methods related to RF, MARS, and ANN; 1982–2013; Jung et al., 2017) and LUE-based GPP product from MODIS (V55; 2000–2015; Zhao & Running, 2010). We then compared CCW GPP with these data spatially. Annul land sink from Global Carbon Budget (Le Quéré et al., 2018) was also obtained to show its association with global GPP by CCW. SIF is a light emission produced by photosynthetic pigments from their excited state and is considered to be linked with GPP (Meroni et al., 2009; Sun et al., 2017). In this study, we further evaluated CCW GPP with SIF from OCO-2 (Sun et al., 2017). OCO-2 is a National Aeronautics and Space Administration mission designed to measure atmospheric CO_2, which was launched in July 2014 (Frankenberg et al., 2014). SIF from OCO-2 is measured at the wavelengths of

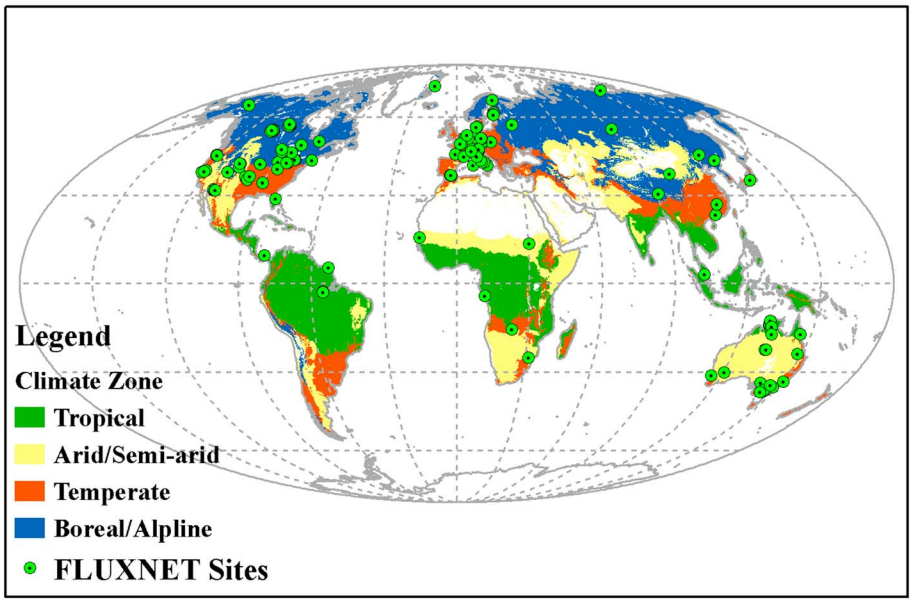

Figure 1. Spatial distributions of FLUNXNET2015 sites and climate zones derived from Köppen-Geiger climate classification.

757 and 771 nm. The daily level-2 SIF-lite data in the year of 2015 were compiled to global monthly data at the spatial resolution of 1° × 1° (Sun et al., 2018). It is noted that only high-quality data after a series of screenings under the nadir view were used, and the sufficient number of soundings in each monthly bin ensured a robust signal of the grid-average SIF (Sun et al., 2018). The monthly SIF was derived from the corrected SIF at two wavelengths:

$$SIF = (SIF_{757\text{nm}} + 1.5{\times}SIF_{771\text{nm}})/2.0 \quad (2)$$

To match the coarse resolution of OCO-2 SIF, global monthly GPP by CCW were rescaled to 1° × 1°, and pixels with low quality of SIF were masked out in the comparison.

2.5. Simulation Design

To disentangle the effects of VCC and climate change on GPP, three groups of simulation scenarios were designed based on different combinations of inputs to CCW (Table 1; Zhang et al., 2014). Group I was used to quantify VCC effect on GPP by allowing both land cover and fraction of photosynthetically active radiation (FPAR) to change along with time while keeping climate factors constant at the initial level of 2,000. Note that in CCW, FPAR is related to vegetation greenness as measured by NDVI, while land cover determines the biome-specific potential LUE and its sensitivity to climate. Therefore, VCC here represents the combined effects of vegetation abundance and vegetation structure/type changes on GPP. Group II was designed to quantify separate, combined, and total effects of three climate factors (i.e., radiation, temperature and VPD) on GPP by keeping land cover and FPAR held at the level of 2,000. Group III was used to account for combined effects of VCC and climate change.

To derive the spatial pattern of major factors controlling GPP, we compared the effects from VCC and climate on annual GPP trend (i.e., linear slope). Four forms of VCC and climate effects based on their signs (i.e., positive and negative) were identified: positive VCC effect (VCC+; largest amplitude of VCC effect with positive sign),

Table 1
Simulation Design to Disentangle the Effects of VCC and Climate Change on GPP by CCW

Group		Land cover	FPAR	Radiation	Temperature	VPD
I	VCC	▲	▲	△	△	△
II	Climate	△	△	▲	▲	▲
		△	△	▲	△	△
		△	△	△	▲	△
		△	△	△	△	▲
		△	△	▲	▲	△
		△	△	▲	△	▲
		△	△	△	▲	▲
III	All	▲	▲	▲	▲	▲

Note. ▲: variable changes along the time; △: variable is held at the initial year of 2000. CCW = Coupled Carbon and Water Model; FPAR = fraction of photosynthetically active radiation; GPP = gross primary production; VCC = vegetation cover change; VPD = vapor pressure deficit.

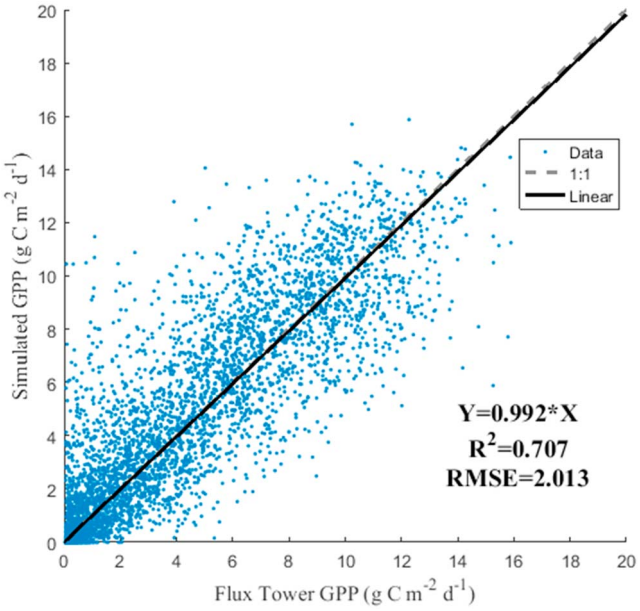

Figure 2. Evaluation of GPP estimated by Coupled Carbon & Water Model with reserved flux-tower derived GPP. GPP = gross primary production; RMSE = root-mean-square error.

negative VCC effect (VCC−; largest amplitude of VCC effect with negative sign), positive climate effect (Climate+; largest amplitude of climate effect with positive sign), and negative climate effect (Climate−; largest amplitude of climate effect with negative sign).

2.6. Published Global Annual GPP and Greenness Trends

To evaluate global annual GPP trend by CCW along with global greenness trend by MODIS vegetation index, we further selected a series of global published GPP models and greenness products (Table S5). These models included the following: ISIMIP2a (1982–2013; Ito et al., 2017), CMIP5a (1982–2011; Smith et al., 2016), BEPS (1982–2015; He et al., 2017), BESS (2000–2015; Jiang & Ryu, 2016), VPM (2000–2015; Zhang, Xiao, et al., 2017), and MOD17-GIMMS (1982-2011; Smith et al., 2016). Overall, the models used for trend evaluation were grouped as three types: (1) machine-learning based (i.e., FLUXCOM), (2) LUE based (i.e., MOD17, MOD17-GIMMS, and VPM), and (3) process based (ISIMIP2a, CMIP5a, BESS, and BEPS). Besides MODIS-C6 NDVI/EVI, global long-term NDVI products from GIMMS3g (V1; 1982–2000) and VIP (V4; 1982–2000), and global LAI products from MODIS-C6 (2000–2015), TCDR (1982–2000), and GIMMS3g (V1; 1982–2000; Jiang et al., 2017) were also included to evaluate global greenness change. The AVHRR-based global NDVI and LAI products were used to quantify global greenness trend from 1982 to 2000, while MODIS-C6 EVI/LAI were used for trend analysis from 2000 to 2015.

3. Results

3.1. Evaluation of CCW Model

The comparison of reserved flux data and modeled GPP showed a generally good performance of CCW, which captured 71% of variations in GPP ($P < 0.001$) with a root-mean-square error of 2.0 g C·m^{-2}·day^{-1} (Figure 2). This recalibration showed a slightly better performance than the initial version of CCW with R^2 of 0.67 ($P < 0.01$; Zhang et al., 2016). Further assessments of CCW on biome and site levels are displayed in Figure S1. Overall, CCW consistently showed reasonable performances in most sites. The updated CCW was also comparable to a series of existing LUE models reported by Yuan et al. (2014) and a recently modified LUE model developed by Wang et al. (2017) in terms of R^2 and root-mean-square error (Table S6).

Multiyear mean of global annual GPP estimated by CCW from 2000 to 2015 is 133.1 ± 1.2 Pg C/year, which is close to the value of 136 Pg C/year derived from the optical integration of multiple models (Schwalm et al., 2015) and among the broad range of global GPP estimations (i.e., 99–187 Pg C/year; Anav et al., 2015; Schwalm et al., 2015). Spatially, annual GPP estimated by CCW was higher in tropical and temperate regions but lower in boreal/alpine and arid/semiarid regions, consistent with FLUXCOM GPP and MODIS GPP (Figure S2). However, CCW GPP differed from MODIS GPP on regional scales, especially in tropical regions such as Amazonia and Indonesia, and temperate regions such as the southeastern United States, China, and western Europe (Figures S2a and S2b). In these regions, CCW GPP tended to be higher, and their spatial patterns were more consistent with FLUXCOM GPP and MODIS vegetation index (Figures S2c and S2d).

We further evaluated CCW GPP based on OCO-2 SIF. Global GPP from CCW correlated well with seasonal OCO-2 SIF ($R = 0.95$; $P < 0.001$) in 2015 (Figure S3). Spatially, the seasonal maximum SIF from OCO-2 effectively captured the high productive zones for croplands in the Northern Hemisphere, such as the corn belt in the Midwestern United States, European Plain, and China's Northeast Plain (Figure S4b; Guanter et al., 2014). CCW GPP also well detected those high productive regions (Figure S4a). Overall, the spatial pattern of annual GPP by CCW was highly consistent with that of SIF derived from OCO-2 ($R = 0.87$, $P < 0.001$), especially in the tropical regions (Figures S4c and S4d). Therefore, we deem that CCW is robust and appropriate to be used to investigate global GPP dynamics.

3.2. Nonuniform Greening Earth

From 2000 to 2015, terrestrial vegetation showed a greening trend over 74.8% of the vegetated area according to MODIS Terra-C6 NDVI (Figure 3a). About 28.6% of vegetated land exhibited significant greening ($P < 0.05$), while only 5.4% of vegetation showed significant browning ($P < 0.05$). Overall, global vegetation had a greening rate on the order of 0.001 year^{-1} or 0.23%/year (i.e., annual linear trend relative to the year 2000 base; the same definition of relative changing rate for annual trend hereafter) by NDVI ($P < 0.001$). However, the overall greening was nonuniform across the globe (Figure 3a) and along with the base greenness (Figure 3b). Vegetation greening mainly occurred in temperate and boreal zones with median and low base greenness. In contrast, vegetation browning tended to appear in tropical regions with dense vegetation. Overall, boreal/alpine regions, accounting for about 25% of global total greenness, contributed to over 40% of global total increased greenness, while tropical regions with 38% of global total greenness were only responsible for 15% of global increased greenness (Figure S5). The nonuniform vegetation greening-browning pattern may have profound implications in global GPP.

3.3. Climate Warming-Induced Drying and Global Deforestation

Global vegetated land showed a significant warming rate of 0.02 °C/year ($P = 0.02$) based on the annual air temperature from CRU-NCEP. Given a negligible change in total precipitation (−0.78 mm^{-1}·year^{-1}, $P = 0.56$), the warming caused a significant drying trend with an increasing rate of 1.4 Pa/year ($P < 0.001$) in global annual mean VPD (Figure 3c). During the same period, global forest area shrank 12×10^6 ha every 5 years ($P < 0.001$) according to ESA-CCI, which is comparable to the FAO Forest Resource Assessment data (18×10^6 ha forest loss every 5 years during 2000–2015; $P < 0.001$; Figure 3d). Global deforestation was accompanied by the increase of cropland and other nonforest vegetation, especially in the tropical regions (Figure S6).

3.4. Limited GPP Increase Under Climate Change and Vegetation Cover Change

By integrating changes in vegetation cover and climate into CCW model, we estimated a much weaker global GPP trend (0.110 Pg C/year or 0.08%/year; $P = 0.07$; referred to as $GPP_{vctrend}$ here after) when compared with the global greening rate (i.e., 0.23%/year; $P < 0.001$) during the same period (Figures 4a and 4b). Our simulation showed that VCC would increase the global GPP at a rate of 0.235 Pg C/year or 0.18%/year ($P < 0.001$) without climate stress. However, when the effects of climate were considered, global GPP increase was sharply reduced by 53%. Contrary to VCC, climate exerted a strong negative influence on global GPP (i.e., −0.139 Pg C/year or −0.10%/year; $P = 0.03$). Among three climate factors, VPD showed the strongest negative effect on global GPP (−0.140 Pg C/year; $P = 0.02$), while temperature and radiation did not generate statistically significant effects (Figures 4c and 4d). Globally, the negative effect from VPD dominated its interactive effects with the other two factors (Figure 4d). Overall, VCC dominated the overall increasing trend of global GPP, yet climate strongly shaped the interannual variation of global GPP.

Spatially, simulated annual GPP showed upward trends over 60.4% of global vegetated area (17.8% with significant trends, $P < 0.05$; Figure 5a), which were much less than the significant greening extent (Figure 3a). The enhanced GPP mainly occurred in East and South Asia, northwestern North America, central Africa, southwestern South America, and southeastern Australia. Notably, some browning or weak greening areas showed strong GPP reductions, such as central Eurasia, eastern United States, Indochina, and Amazonia. Boreal/alpine regions, accounting for 19% of global total GPP, contributed 47% of global total increased GPP (Figure S5), followed by temperate (38.0%) and arid/semiarid (16.8%) regions (Figure 5b). Nevertheless, the tropics, accounting for over half of global total GPP (Figure S5), was the only region that negatively contributed to global GPP trend (−2.0%; Figure 5b).

Across tropical subregions, tropical Africa and Asia both showed upward trends in annual total GPP, equal to 24.9% and 2.1% of $GPP_{vctrend}$, respectively (Figure 5b). However, tropical America, the only subregion where the negative effect mainly from warming-induced drying was much larger than the weakly positive effect of VCC, exhibited a downward GPP trend (equal to −29% of $GPP_{vctrend}$) and more than offset the total increased GPP from tropical Africa and Asia (equal to 27% of $GPP_{vctrend}$). It is important to note that severe droughts occurred in 2005, 2010, and 2015 across Amazonia (Feldpausch et al., 2016; Jiménez-Muñoz et al., 2016), causing strong negative annual GPP anomalies in tropical America (Figures S7 and S8) and clearly projecting onto the global GPP dynamics (Figure 4a). Overall, the annual GPP trend was most strongly

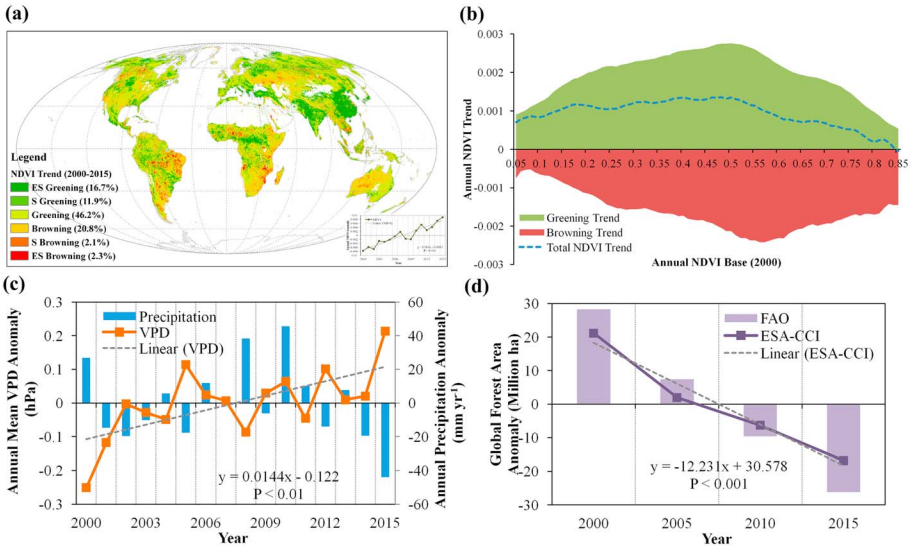

Figure 3. Changes in global vegetation greenness, climate, and forest area over 2000 to 2015. (a) Spatial pattern of linear trend in annual NDVI from Moderate Resolution Imaging Spectroradiometer C6; greening: linear slope of annual NDVI > 0; browning: linear slope of annual NDVI < 0; ES: extremely significant with $P < 0.01$; S: significant with $P < 0.05$; the number in the parenthesis is the browning/greening area relative to global vegetated area; the lower right inset panel shows the interannual variation of global averaged NDVI. (b) Distribution of annual NDVI positive and negative trends, respectively, along the gradient of NDVI base in 2000; the bin size of NDVI (x axis) is 0.01; total NDVI trend indicates the annual NDVI trend for all area within the bin. (c) Annual changes of global averaged total precipitation and VPD from CRU-National Centers for Environmental Prediction. (d) Annual changes of global forest areas derived from FAO Forestry inventory data and ESA-CCI land cover data. All the statistics are calculated over terrestrial vegetated area. All anomalies are relative to their multiple-year averages. FAO = Food and Agriculture Organization; ESA-CCI = European Space Agency-Climate Change Initiative; NDVI = normalized difference vegetation index; VPD = vapor pressure deficit.

influenced by climate in the tropics, followed by temperate, boreal/alpine, and arid/semiarid zones (Figure 5b).

The effects of VCC and climate on GPP differed along the latitudinal gradient (Figure 5c). Although a relatively large greening trend existed in the high latitudes (i.e., >55°N), its actual effect on annual GPP was limited likely due to short growing seasons and relatively strong climate constraints. We further examined the spatial pattern of dominant factors by comparing their direct GPP effects on each pixel (Figure 5d). Overall, the positive effect of VCC dominated annual GPP trend over 49.2% of vegetated area, which were mainly located over the Northern Hemisphere, central Africa, and southeastern Australia (Figure 5d). A certain portion of the vegetated area (18.5%) showed negative GPP controls by VCC, which were mainly clustered in the Southern Hemisphere and midlatitudes Eurasia (Figure 5d). Climate had positive effects on GPP over 11.6% of vegetated surface, which were scattered in boreal zone due to climate warming, and central Africa and South America due to wetting trends (Figures 5d, S9, and S10). However, 20.7% of the vegetated area, nearly twice the area with positive effect, showed negative climate effects on GPP (largely due to warming-induced VPD increase; Figures S9 and S10), which were mainly distributed in Amazonia, southeastern United States, central Eurasia, and Indochina (Figure 5d).

3.5. Negative Contribution of Tropical Forests in Global GPP Increase

During the study period, global total increased GPP were mainly contributed by nonforests with an annual rate of 0.137 Pg C/year (equal to 124.6% of $GPP_{vctrend}$; Figure 6a). On the contrary, global forests negatively contributed to annual global GPP trend with a rate of −0.027 Pg C/year (or −24.6% of $GPP_{vctrend}$). Further analysis showed that forests in tropical America and Asia had remarkable GPP reductions (−0.082 Pg C/year or −74.6% of $GPP_{vctrend}$), which more than offset forest GPP increases from tropical Africa and other nontropical zones (0.055 Pg C/year or 49.9% of $GPP_{vctrend}$; Figure 6a). The forest GPP reductions in tropical America and Asia were largely due to deforestation (Figures 6b and S6) and climate stresses (Figures 5, S7, and S9). Among nonforest types, cropland contributed most to the annual total GPP increase (51%), followed by woody savanna (33%) and grassland (11%; Figure 6b). The enhanced cropland GPP, which were partly

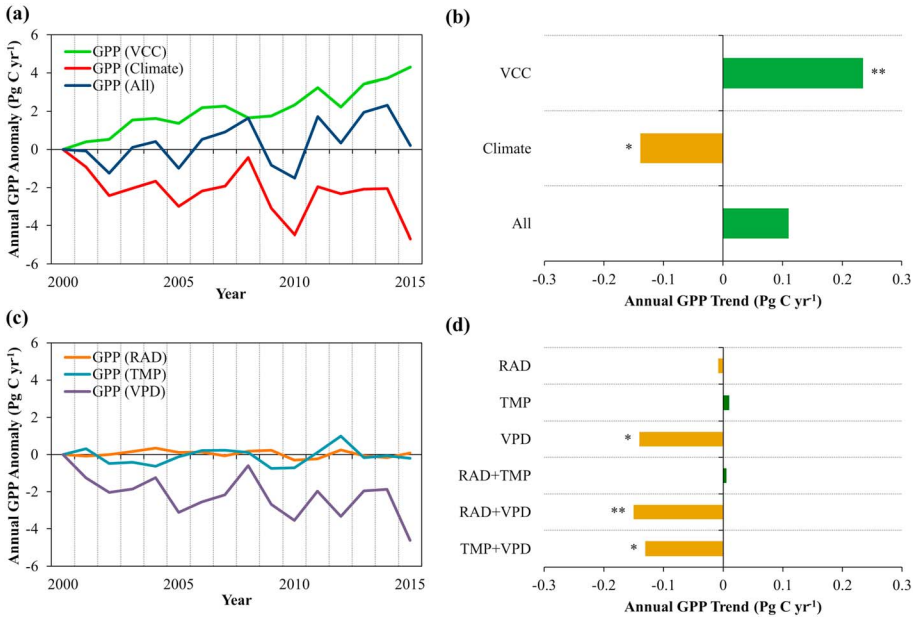

Figure 4. Effects of vegetation cover change (VCC) and climate change on interannual variations and trends in global gross primary production (GPP) from 2000 to 2015. (a) Annual changes of global GPP when considering VCC and climate change, respectively. (b) Annual global GPP trends contributed by factors in (a). (c) Annual changes of global GPP caused by three climate factors including radiation (RAD), temperature (TMP), and vapor pressure deficit (VPD). (d) Annual trends in global GPP contributed by climate factors in (c) and their interactive effects. All the statistics are calculated over terrestrial vegetated area. The annual anomaly is relative to the initial year of 2000. Statistical significance level *(P)*: * ($P < 0.05$), ** ($P < 0.01$).

due to the active management and agricultural expansion (Figure S6), were widely distributed across different climate zones except boreal region (Figure 6b).

4. Discussion

Global vegetation showed a significant greening trend from 2000 to 2015 based on MODIS-C6 vegetation index products (Figures 4a and 7a). By only considering the VCC effect in CCW, our model results showed a significant increase in global GPP (Figure 4). However, when further accounting for climate effects, the greening effect was considerably offset by 53% and a much weaker increase in global GPP was found when compared with the global greening rate (Figure 7a), which rejects our initial hypothesis on the proportional increase of global GPP along with Earth's greening. Vegetation index based on optical remote sensing is a robust indicator of leaf chlorophyll abundance, which is closely linked to the photosynthesis capacity and plant growth activity (Myneni et al., 1995; Running et al., 2000). However, the vegetation index is not a proxy of GPP as there are a set of climatic factors limiting the conversion of absorbed sunlight to sequestered carbon (Chapin et al., 2002; Potter et al., 1993; Running et al., 2000; Zhao & Running, 2010). Meteorological records showed that the early period of this century was the warmest since 1880s (Trenberth, 2015). Our simulations confirmed that the warming-induced drying in terms of increased VPD was the major factor governing the negative climatic effects on GPP (Figures 4 and 5).

During the study period, ML-based global GPP estimations from FLUXCOM showed no particular trends, while a series of process-based models considering the CO_2 fertilization effect exhibited a stronger trend than CCW (Figure 7a). Evidences from the free-air CO_2 enrichment data suggested that the CO_2 fertilization effect might be much overestimated by current process-based models, largely due to a lack of representation of nutrient constraints (He et al., 2017), potential climate feedbacks (Smith et al., 2016), or the acclimation of plants to CO_2 fertilization (Ainsworth & Rogers, 2007). For example, a 20-year free-air CO_2 enrichment experiment carried out in temperate grasslands showed that the CO_2 fertilization effect on C_3 plants was negligible after 15 to 20 years (Reich et al., 2018), suggesting that plant response to CO_2 may depend on time, species traits and resource availability (Körner, 2006; Nowak et al., 2004; Terrer et al., 2018).

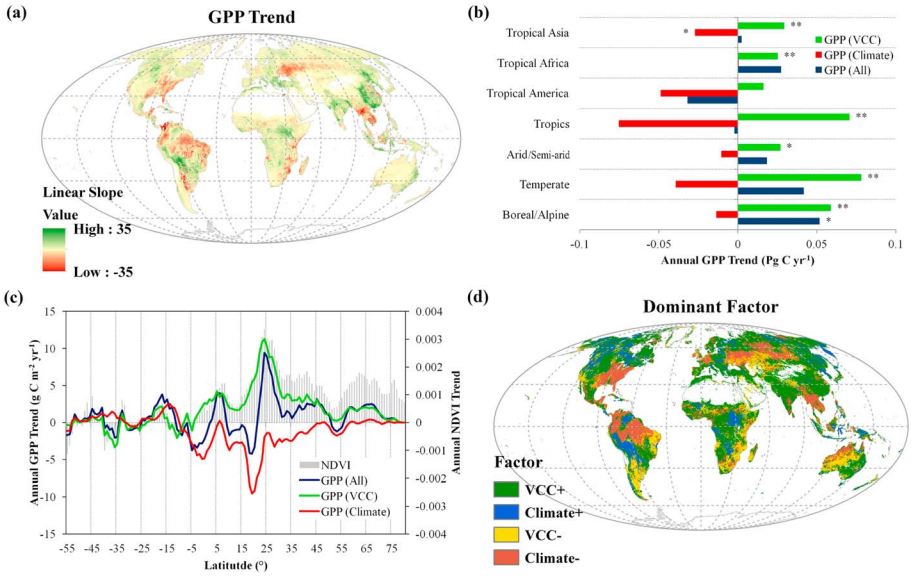

Figure 5. Spatial pattern of global GPP trend and its dominant factors from 2000 to 2015. (a) Spatial pattern of linear trend in annual global GPP by coupled carbon and water. (b) Annual global GPP trends caused by VCC and climate change in different climate zones. Statistical significance level (P): * ($P < 0.05$), ** ($P < 0.01$). (c) Changes of annual NDVI trend and global GPP trends influenced by different factors along the latitudinal gradient (latitude internal: 1°). (d) Spatial pattern of dominant factors that controlling global GPP trend; + refers to positive effect, and − negative effect. Global unvegetated area in (a) and (d) are masked out, and all relevant statistics are based on vegetated area. GPP = gross primary production; NDVI = normalized difference vegetation index; VCC = vegetation cover change.

Annual GPP trend by CCW was stronger than MODIS GPP, probably because the latter suffered from the sensor degradation effect in MODIS-C5 data (Lyapustin et al., 2014). However, VPM, another LUE-based model, which used the MODIS-C6 data (Zhang, Xiao, et al., 2017), showed a much stronger trend than CCW and even process-based models (Figure 7a). The annual GPP variation by VPM was actually very similar to CCW by only accounting for VCC effect ($R = 0.934$, $P < 0.001$; Figure S11). Given VPM is not a strictly calibrated model based on in situ observation data, the parameters especially those related to FPAR and water stress scalar may have uncertainties (Zhang, Xiao, et al., 2017). In spite of that, all models showed relatively weak annual GPP trends when compared with the annual greening rate in terms of MODIS-C6 LAI (Figure 7a). This pattern was consistent even extending back to the year of 1982 (Figure 7b). According to the theory of LUE model (Potter et al., 1993), the potential LUE realized by plants without environmental stresses, which is closely linked with remote-sensed greenness, could provide the upper limit for GPP estimation (Ryu et al., 2019).

CCW model was calibrated based on global flux tower data and MODIS-C6 data. However, it showed relatively poor performance in some forest, woody savanna and cropland sites (Figure S1), which may be related to the uncertainties from both flux data and MODIS data, their potential footprint mismatches, and/or the sensitivity and representation of model environmental scalars (Jung et al., 2011; Tramontana et al., 2016). Plant's water stress is codominated by soil water supply (i.e., soil water content) and atmospheric water demand (i.e., VPD). However, the effect of soil water content was not directly modeled in CCW. Although VPD and soil moisture are better coupled at monthly time steps (Novick et al., 2016) and the data-driven method used in this study could implicitly incorporate this covariance (Zhang et al., 2015; Zhang et al., 2016), the sensitivity of LUE to VPD may vary along with soil moisture gradients (Novick et al., 2016), which is worthy of being investigated and included in CCW in the future. In this study, we conducted model simulations to separate the effects of VCC and climate on GPP. However, VCC is further influenced by climate change/variation (Figure S12; Zhang, Song, et al., 2017), and such influences are difficult to separate by CCW. Therefore, the climate effect on GPP identified in our study may be underestimated. The process-based model such as Dynamic Global Vegetation Model (Fisher et al., 2018) may help to address this issue in the future.

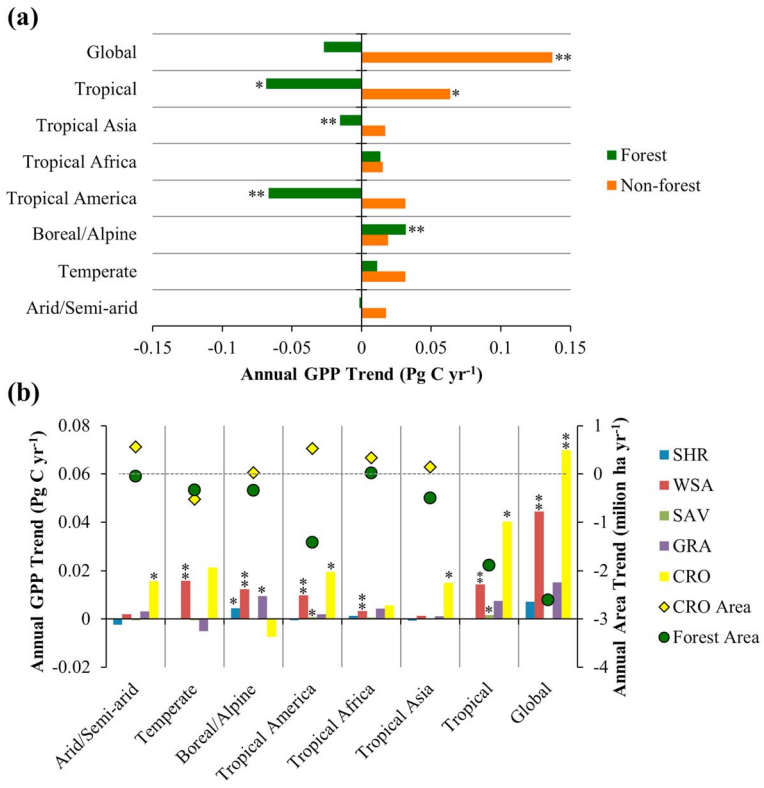

Figure 6. Contributions of forests and nonforests in global GPP trend from 2000 to 2015. (a) Annual GPP trends contributed by forests and nonforests over different zones. (b) Annual GPP trends contributed by nonforests, and annual changing rates of cropland and forest area from European Space Agency-Climate Change Initiative over different zones; forests here include broadleaf, deciduous leaf, and mixed forests, while nonforests include cropland (CRO), shrub (SHR), savanna (SAV), woody savanna (WSA), and grassland (GRA). Statistical significance level (P): * ($P < 0.05$), ** ($P < 0.01$).

Prior research reported a climate-driven increase in terrestrial vegetation production from 1982 to 1999 (Nemani et al., 2003). In this study, we showed a continuation of the increasing vegetation production since 2000 (Figure 4). However, the recent enhanced GPP were mainly contributed by boreal and temperate regions where a widespread greening and climate warming occurred (Dass et al., 2016). Tropical regions, once a major driver of the increased global vegetation production (Nemani et al., 2003), negatively contributed to global GPP due to warming-induced moisture stress and deforestation during the study period (Figures 4, 5, S6, and S10). Tropical GPP declines were also highlighted by other recent studies (Baccini et al., 2017; Bastos et al., 2018; Liu et al., 2017; Smith et al., 2016). Therefore, although a substantial greening occurred on the Earth surface from 2000 to 2015, a proportional global enhanced gross carbon sequestration was not found (Figures 4 and 5), which appeared to be further responsible for the weak increased land carbon sink during the same period (i.e., 0.04 Pg C/year, $P > 0.05$; Figure S11).

General Circulation Models project a large future rainfall variability and more frequent droughts in the tropical regions (Fu, 2015; Lewis et al., 2011). Given the sensitivity of tropical forests to drought revealed in this study (Figures 5, S7, and S10) as well as other independent studies (Li et al., 2017; Rowland et al., 2015; Schwalm et al., 2017), these hydroclimate changes are likely to significantly influence tropical ecosystem productivity, thus a major mechanism to alter global carbon cycle (Baccini et al., 2017; Liu et al., 2017; Madani et al., 2018). From 2000 to 2015, global enhanced GPP were largely contributed by nonforests, especially cropland (Figure 6). A recent study based on MODIS LAI also showed that global greening is mainly driven by cropland (Chen et al., 2019). However, given the limited potential of carbon storage from croplands due to harvest and consumption (Wolf et al., 2015), GPP increase in croplands at the cost of GPP reduction in forests may have significantly shifted the distribution of land carbon sink and the role of vegetated land as a carbon sink may be weakened or even reversed in the future (Jones et al., 2018; Molotoks et al., 2018).

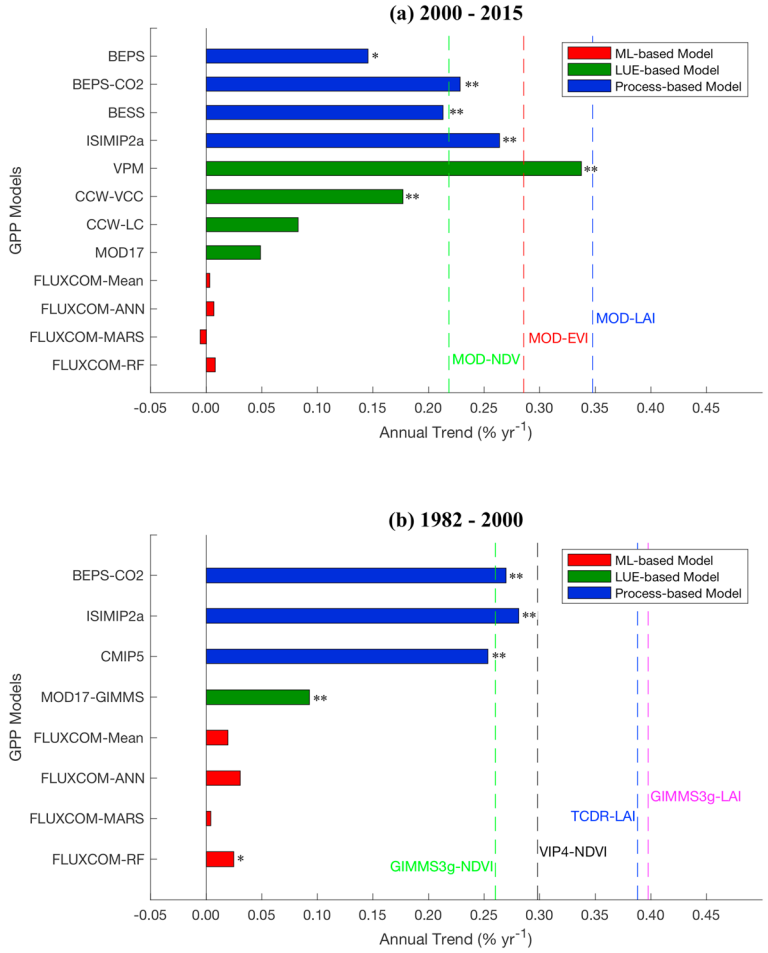

Figure 7. Trend comparisons in global annual GPP and greenness from different data sources (a) from 2000 to 2015 and (b) from 1982 to 2000. Three groups of GPP models were included: ML based (i.e., FLUXCOM), LUE based (i.e., CCW, MOD17, MOD17-GIMMS, and VPM), and process based (ISIMIP2a, CMIP5, BEPS, and BESS). The vertical dash lines indicate global greenness changing rates shown by different indicators. Global averaged greenness in (a) included MODIS-C6 NDVI, EVI, and LAI. Global averaged greenness in (b) included GIMMS3g NDVI, VIP4 NDVI, GIMMS3g LAI, and TCDR LAI. All trends in annual GPP and greenness were scaled by their multiple-year means. FLUXCOM-Mean in (a) was the mean of FLUXCOM-ANN, −MARS and −RF from 2000 to 2013. MOD17-GIMMS and CMIP5 in (b) were from 1982 to 2011. BEPS-CO_2 was the GPP estimation only accounting for CO_2 fertilization, while BEPS was further accounted by nitrogen constraint (He et al., 2017). * $P < 0.05$; ** $P < 0.01$. CCW = coupled carbon and water; GPP = gross primary production; ML = machine learning; LUE = light-use efficiency; LAI = leaf area index; NDVI = normalized difference vegetation index.

Our findings have significant implications on the ongoing commitment in mitigating global warming through carbon sequestration. Countries have pledged to take actions to limit future global warming within 2 °C from the preindustrial temperature by 2100 at the Paris Summit (Tollefson, 2015). Our analysis implies that global terrestrial ecosystems are still important but their capacity in sequestering atmospheric CO_2 may diminish under climate and land use changes. Therefore, more rigorous anthropogenic emission reduction and renewed efforts for forest conservation and land management that enhance carbon sequestration (Canadell & Raupach, 2008; Davies-Barnard et al., 2015) are likely needed in a warmer world.

5. Conclusions

The Earth's terrestrial biosphere is greening, but how it is linked with terrestrial gross carbon sequestration is not quite clear. In this study, based on a calibrated remote sensing-driven model, we investigated terrestrial GPP dynamics in the context of VCC and climate change from 2000 to 2015. We found a much

weaker increase in global GPP (0.08%/year; $P = 0.07$) when compared with the global greening rate (0.23%/year; $P < 0.001$). Model simulations showed that such a mismatch between global GPP and greenness trends was mainly caused by climate stress. Further analysis by biome indicated that the generally enhanced global GPP was mainly contributed by cropland and other nonforest biomes, while global forests, especially in tropical regions, negatively contributed to global GPP trend. Given the limited potential of carbon storage from cropland, the contrasting GPP changes (i.e., cropland GPP increase vs. forest GPP reduction) may have shifted the distribution of the land carbon sink. Our study suggests that the capacity of terrestrial gross carbon sequestration may be weakened under climate and land use changes, which has important implications in the global carbon cycle and climate warming mitigation.

Acknowledgments

We acknowledged NASA Science Teams for providing MODIS data and OCO-2 SIF data, ESA CCI for providing global land cover data, Dr. Maosheng Zhao from NASA/GSFC for providing MODIS GPP data, Dr. Martin Jung from Max Planck Institute for Biogeochemistry for providing FLUXCOME GPP data, Dr. Liming He from University of Toronto for providing BEPS GPP data, Dr. Akihiko Ito from NIES for providing ISIMIP2a data, Dr. Chongya Jiang and Dr. Youngryel Ryu from Seoul National University for providing BESS data and relevant greenness data, Dr. Nicolas Viovy from LSCE for providing the global CRU-NCEP climate data, and Dr. Ying Sun from Cornell University for assisting in processing OCO-2 SIF data. We also acknowledge the global eddy covariance flux data provided by FLUXNET, a global network of micrometeorological tower sites gathered from a series of regional networks including CarboeuropeIP, AmeriFlux, Fluxnet-Canada, LBA, Asiaflux, Chinaflux, USCCC, Ozflux, Carboafrica, Koflux, NECC, TCOS-Siberia, and AfriFlux (http://www.fluxdata.org/). All other data providers cited but not listed here were also appreciated. This work was supported by the NASA Carbon Cycle Science (NNX17AE69G), U.S. National Science Foundation (DEB-1313756), and Natural Science Foundation of China (31528004). All data needed to evaluate the conclusions are present in the paper and/or the Supporting Information. The generated global GPP data set by CCW can be accessed from Dr. Yulong Zhang's research website (https://sites.google.com/view/planetlab/download). The authors declare no competing interests.

References

Ainsworth, E. A., & Rogers, A. (2007). The response of photosynthesis and stomatal conductance to rising [CO2]: mechanisms and environmental interactions. *Plant, cell & environment*, *30*(3), 258–270. https://doi.org/10.1111/j.1365-3040.2007.01641.x

Anav, A., Friedlingstein, P., Beer, C., Ciais, P., Harper, A., Jones, C., et al. (2015). Spatiotemporal patterns of terrestrial gross primary production: A review. *Reviews of Geophysics*, *53*, 785–818. https://doi.org/10.1002/2015RG000483

Anav, A., Friedlingstein, P., Kidston, M., Bopp, L., Ciais, P., Cox, P., et al. (2013). Evaluating the land and ocean components of the global carbon cycle in the CMIP5 Earth System Models. *Journal of Climate*, *26*(18), 6801–6843. https://doi.org/10.1175/JCLI-D-12-00417.1

Anderegg, W., Schwalm, C., Biondi, F., Camarero, J. J., Koch, G., Litvak, M., et al. (2015). Pervasive drought legacies in forest ecosystems and their implications for carbon cycle models. *Science*, *349*(6247), 528–532. https://doi.org/10.1126/science.aab1833

Baccini, A., Walker, W., Carvalho, L., Farina, M., Sulla-Menashe, D., & Houghton, R. (2017). Tropical forests are a net carbon source based on aboveground measurements of gain and loss. *Science*, *358*(6360), 230–234. https://doi.org/10.1126/science.aam5962

Bastos, A., Friedlingstein, P., Sitch, S., Chen, C., Mialon, A., Wigneron, J.-P., et al. (2018). Impact of the 2015/2016 El Niño on the terrestrial carbon cycle constrained by bottom-up and top-down approaches. *Philosophical Transactions of the Royal Society B: Biological Sciences*, *373*(1760). https://doi.org/10.1098/rstb.2017.0304

Beer, C., Reichstein, M., Tomelleri, E., Ciais, P., Jung, M., Carvalhais, N., et al. (2010). Terrestrial gross carbon dioxide uptake: Global distribution and covariation with climate. *Science*, *329*(5993), 834–838. https://doi.org/10.1126/science.1184984

Campbell, J., Berry, J., Seibt, U., Smith, S. J., Montzka, S., Launois, T., et al. (2017). Large historical growth in global terrestrial gross primary production. *Nature*, *544*(7648), 84–87. https://doi.org/10.1038/nature22030

Canadell, J. G., & Raupach, M. R. (2008). Managing forests for climate change mitigation. *Science*, *320*(5882), 1456–1457. https://doi.org/10.1126/science.1155458

Chapin, F. III, Matson, P., & Mooney, H. (2002). *Principles of terrestrial ecosystem ecology* (pp. 298–300). New York, USA: Springer-Verlag.

Chen, C., Park, T., Wang, X., Piao, S., Xu, B., Chaturvedi, R. K., et al. (2019). China and India lead in greening of the world through land-use management. *Nature Sustainability*, *2*(2), 122–129. https://doi.org/10.1038/s41893-019-0220-7

Ciais, P., Reichstein, M., Viovy, N., Granier, A., Ogée, J., Allard, V., et al. (2005). Europe-wide reduction in primary productivity caused by the heat and drought in 2003. *Nature*, *437*(7058), 529–533. https://doi.org/10.1038/nature03972

Cramer, W., Bondeau, A., Schaphoff, S., Lucht, W., Smith, B., & Sitch, S. (2004). Tropical forests and the global carbon cycle: Impacts of atmospheric carbon dioxide, climate change and rate of deforestation. *Philosophical Transactions of the Royal Society B: Biological Sciences*, *359*(1443), 331–343. https://doi.org/10.1098/rstb.2003.1428

Dass, P., Rawlins, M. A., Kimball, J. S., & Kim, Y. (2016). Environmental controls on the increasing GPP of terrestrial vegetation across northern Eurasia. *Biogeosciences*, *13*(1), 45–62. https://doi.org/10.5194/bg-13-45-2016

Davies-Barnard, T., Valdes, P., Singarayer, J. S., Wiltshire, A., & Jones, C. (2015). Quantifying the relative importance of land cover change from climate and land use in the representative concentration pathways. *Global Biogeochemical Cycles*, *29*, 842–853. https://doi.org/10.1002/2014GB004949

Didan, K., Munoz, A. B., Solano, R., & Huete, A. (2015). *MODIS vegetation index user's guide (MOD13 Series)* (pp. 1–38). The University of Arizona: Vegetation Index and Phenology Lab.

Feldpausch, T., Phillips, O., Brienen, R., Gloor, E., Lloyd, J., Lopez-Gonzalez, G., et al. (2016). Amazon forest response to repeated droughts. *Global Biogeochemical Cycles*, *30*, 964–982. https://doi.org/10.1002/2015GB005133

Fisher, R. A., Koven, C. D., Anderegg, W. R., Christoffersen, B. O., Dietze, M. C., Farrior, C. E., & Lichstein, J. W. (2018). Vegetation demographics in Earth System Models: A review of progress and priorities. *Global Change Biology*, *24*(1), 35–54. https://doi.org/10.1111/gcb.13910

Frankenberg, C., O'Dell, C., Berry, J., Guanter, L., Joiner, J., Köhler, P., et al. (2014). Prospects for chlorophyll fluorescence remote sensing from the Orbiting Carbon Observatory-2. *Remote Sensing of Environment*, *147*, 1–12. https://doi.org/10.1016/j.rse.2014.02.007

Fu, R. (2015). Global warming-accelerated drying in the tropics. *Proceedings of the National Academy of Sciences*, *112*, 3593–3594.

Guanter, L., Zhang, Y., Jung, M., Joiner, J., Voigt, M., Berry, J. A., et al. (2014). Global and time-resolved monitoring of crop photosynthesis with chlorophyll fluorescence. *Proceedings of the National Academy of Sciences*, *111*(14), E1327–E1333. https://doi.org/10.1073/pnas.1320008111

He, L., Chen, J. M., Croft, H., Gonsamo, A., Luo, X., Liu, J., et al. (2017). Nitrogen availability dampens the positive impacts of CO_2 fertilization on terrestrial ecosystem carbon and water cycles. *Geophysical Research Letters*, *44*, 11,590–11,600. https://doi.org/10.1002/2017GL075981

Hilker, T., Coops, N. C., Wulder, M. A., Black, T. A., & Guy, R. D. (2008). The use of remote sensing in light use efficiency based models of gross primary production: A review of current status and future requirements. *Science of the Total Environment*, *404*(2-3), 411–423. https://doi.org/10.1016/j.scitotenv.2007.11.007

Houghton, R. (2007). Balancing the global carbon budget. *Annual Review of Earth and Planetary Sciences*, *35*(1), 313–347. https://doi.org/10.1146/annurev.earth.35.031306.140057

Ito, A., Nishina, K., Reyer, C. P., François, L., Henrot, A.-J., Munhoven, G., et al. (2017). Photosynthetic productivity and its efficiencies in ISIMIP2a biome models: benchmarking for impact assessment studies. *Environmental Research Letters*, *12*(8), 085001. https://doi.org/10.1088/1748-9326/aa7a19

Jiang, C., & Ryu, Y. (2016). Multi-scale evaluation of global gross primary productivity and evapotranspiration products derived from Breathing Earth System Simulator (BESS). *Remote Sensing of Environment*, *186*, 528–547. https://doi.org/10.1016/j.rse.2016.08.030

Jiang, C., Ryu, Y., Fang, H., Myneni, R., Claverie, M., & Zhu, Z. (2017). Inconsistencies of interannual variability and trends in long-term satellite leaf area index products. *Global Change Biology*, *23*(10), 4133–4146. https://doi.org/10.1111/gcb.13787

Jiménez-Muñoz, J. C., Mattar, C., Barichivich, J., Santamaría-Artigas, A., Takahashi, K., Malhi, Y., et al. (2016). Record-breaking warming and extreme drought in the Amazon rainforest during the course of El Niño 2015–2016. *Scientific Reports*, *6*(1). https://doi.org/10.1038/srep33130

Jones, A. D., Calvin, K. V., Shi, X., Di Vittorio, A. V., Bond-Lamberty, B., Thornton, P. E., & Collins, W. D. (2018). Quantifying human-mediated carbon cycle feedbacks. *Geophysical Research Letters*, *45*, 11,370–11,379. https://doi.org/10.1029/2018GL079350

Jung, M., Reichstein, M., Margolis, H. A., Cescatti, A., Richardson, A. D., Arain, M. A., et al. (2011). Global patterns of land-atmosphere fluxes of carbon dioxide, latent heat, and sensible heat derived from eddy covariance, satellite, and meteorological observations. *Journal of Geophysical Research*, *116*, G00J07. https://doi.org/10.1029/2010JG001566

Jung, M., Reichstein, M., Schwalm, C. R., Huntingford, C., Sitch, S., Ahlström, A., et al. (2017). Compensatory water effects link yearly global land CO2 sink changes to temperature. *Nature*, *541*(7638), 516–520. https://doi.org/10.1038/nature20780

Körner, C. (2006). Plant CO_2 responses: An issue of definition, time and resource supply. *New phytologist*, *172*(3), 393–411. https://doi.org/10.1111/j.1469-8137.2006.01886.x

Le Quéré, C., Andrew, R. M., Friedlingstein, P., Sitch, S., Hauck, J., Pongratz, J., et al. (2018). Global carbon budget 2018. *Earth System Science Data*, *10*(4), 2141–2194. https://doi.org/10.5194/essd-10-2141-2018

Lewis, S. L., Brando, P. M., Phillips, O. L., van der Heijden, G. M., & Nepstad, D. (2011). The 2010 amazon drought. *Science*, *331*(6017), 554–554. https://doi.org/10.1126/science.1200807

Li, Y., Guan, K., Gentine, P., Konings, A. G., Meinzer, F. C., Kimball, J. S., et al. (2017). Estimating global ecosystem isohydry/anisohydry using active and passive microwave satellite data. *Journal of Geophysical Research: Biogeosciences*, *122*, 3306–3321. https://doi.org/10.1002/2017JG003958

Lieth, H., & Whittaker, R. H. (2012). *Primary productivity of the biosphere*. Berlin Heidelberg, New York: Springer Science & Business Media.

Liu, J., Bowman, K. W., Schimel, D. S., Parazoo, N. C., Jiang, Z., Lee, M., et al. (2017). Contrasting carbon cycle responses of the tropical continents to the 2015–2016 El Niño. *Science*, *358*(6360). https://doi.org/10.1126/science.aam5690

Lyapustin, A., Wang, Y., Xiong, X., Meister, G., Platnick, S., Levy, R., et al. (2014). Scientific impact of MODIS C5 calibration degradation and C6+ improvements. *Atmospheric Measurement Techniques*, *7*(12), 4353–4365. https://doi.org/10.5194/amt-7-4353-2014

Madani, N., Kimball, J. S., Ballantyne, A. P., Affleck, D. L., Bodegom, P. M., Reich, P. B., et al. (2018). Future global productivity will be affected by plant trait response to climate. *Scientific reports*, *8*(1), 2870. https://doi.org/10.1038/s41598-018-21172-9

Malhi, Y., Roberts, J. T., Betts, R. A., Killeen, T. J., Li, W., & Nobre, C. A. (2008). Climate change, deforestation, and the fate of the Amazon. *Science*, *319*(5860), 169–172. https://doi.org/10.1126/science.1146961

Meroni, M., Rossini, M., Guanter, L., Alonso, L., Rascher, U., Colombo, R., & Moreno, J. (2009). Remote sensing of solar-induced chlorophyll fluorescence: Review of methods and applications. *Remote Sensing of Environment*, *113*(10), 2037–2051. https://doi.org/10.1016/j.rse.2009.05.003

Molotoks, A., Stehfest, E., Doelman, J., Albanito, F., Fitton, N., Dawson, T. P., & Smith, P. (2018). Global projections of future cropland expansion to 2050 and direct impacts on biodiversity and carbon storage. *Global Change Biology*, *24*(12), 5895–5908. https://doi.org/10.1111/gcb.14459

Myneni, R. B., Hall, F. G., Sellers, P. J., & Marshak, A. L. (1995). The interpretation of spectral vegetation indexes. *IEEE Transactions on Geoscience and Remote Sensing*, *33*(2), 481–486. https://doi.org/10.1109/TGRS.1995.8746029

Nemani, R. R., Keeling, C. D., Hashimoto, H., Jolly, W. M., Piper, S. C., Tucker, C. J., et al. (2003). Climate-driven increases in global terrestrial net primary production from 1982 to 1999. *Science*, *300*(5625), 1560–1563. https://doi.org/10.1126/science.1082750

Novick, K. A., Ficklin, D. L., Stoy, P. C., Williams, C. A., Bohrer, G., Oishi, A. C., et al. (2016). The increasing importance of atmospheric demand for ecosystem water and carbon fluxes. *Nature Climate Change*, *6*(11), 1023–1027. https://doi.org/10.1038/nclimate3114

Nowak, R. S., Ellsworth, D. S., & Smith, S. D. (2004). Functional responses of plants to elevated atmospheric CO_2—Do photosynthetic and productivity data from FACE experiments support early predictions? *New phytologist*, *162*(2), 253–280. https://doi.org/10.1111/j.1469-8137.2004.01033.x

Pettorelli, N., Vik, J. O., Mysterud, A., Gaillard, J.-M., Tucker, C. J., & Stenseth, N. C. (2005). Using the satellite-derived NDVI to assess ecological responses to environmental change. *Trends in ecology & evolution*, *20*(9), 503–510. https://doi.org/10.1016/j.tree.2005.05.011

Pinzon, J. E., & Tucker, C. J. (2014). A non-stationary 1981–2012 AVHRR NDVI3g time series. *Remote Sensing*, *6*(8), 6929–6960. https://doi.org/10.3390/rs6086929

Potter, C. S., Randerson, J. T., Field, C. B., Matson, P. A., Vitousek, P. M., Mooney, H. A., & Klooster, S. A. (1993). Terrestrial ecosystem production: A process model based on global satellite and surface data. *Global Biogeochemical Cycles*, *7*(4), 811–841. https://doi.org/10.1029/93GB02725

Reich, P. B., Hobbie, S. E., Lee, T. D., & Pastore, M. A. (2018). Unexpected reversal of C3 versus C4 grass response to elevated CO_2 during a 20-year field experiment. *Science*, *360*(6386), 317–320. https://doi.org/10.1126/science.aas9313

Rowland, L., da Costa, A. C. L., Galbraith, D. R., Oliveira, R., Binks, O. J., Oliveira, A., et al. (2015). Death from drought in tropical forests is triggered by hydraulics not carbon starvation. *Nature*, *528*(7580), 119–122. https://doi.org/10.1038/nature15539

Running, S. W. (2012). A measurable planetary boundary for the biosphere. *Science*, *337*(6101), 1458–1459. https://doi.org/10.1126/science.1227620

Running, S. W., Nemani, R. R., Heinsch, F. A., Zhao, M., Reeves, M., & Hashimoto, H. (2004). A continuous satellite-derived measure of global terrestrial primary production. *Bioscience*, *54*(6), 547–560. https://doi.org/10.1641/0006-3568(2004)054[0547:ACSMOG]2.0.CO;2

Running, S. W., Thornton, P. E., Nemani, R., & Glassy, J. M. (2000). Global terrestrial gross and net primary productivity from the Earth Observing System. *Methods in ecosystem science*, *3*, 44–45.

Ryu, Y., Berry, J. A., & Baldocchi, D. D. (2019). What is global photosynthesis? History, uncertainties and opportunities. *Remote Sensing of Environment*, *223*, 95–114. https://doi.org/10.1016/j.rse.2019.01.016

Schwalm, C. R., Anderegg, W. R., Michalak, A. M., Fisher, J. B., Biondi, F., Koch, G., et al. (2017). Global patterns of drought recovery. *Nature*, *548*(7666), 202–205. https://doi.org/10.1038/nature23021

Schwalm, C. R., Huntzinger, D. N., Fisher, J. B., Michalak, A. M., Bowman, K., Ciais, P., et al. (2015). Toward "optimal" integration of terrestrial biosphere models. *Geophysical Research Letters*, *42*, 4418–4428. https://doi.org/10.1002/2015GL064002

Sims, D. A., Luo, H., Hastings, S., Oechel, W. C., Rahman, A. F., & Gamon, J. A. (2006). Parallel adjustments in vegetation greenness and ecosystem CO_2 exchange in response to drought in a Southern California chaparral ecosystem. *Remote Sensing of Environment*, *103*(3), 289–303. https://doi.org/10.1016/j.rse.2005.01.020

Smith, W. K., Reed, S. C., Cleveland, C. C., Ballantyne, A. P., Anderegg, W. R., Wieder, W. R., et al. (2016). Large divergence of satellite and Earth system model estimates of global terrestrial CO_2 fertilization. *Nature climate change*, *6*(3), 306–310. https://doi.org/10.1038/nclimate2879

Song, C., Chen, J. M., Hwang, T., Gonsamo, A., Croft, H., Zhang, Q., et al. (2015). Ecological characterization of vegetation using multi-sensor remote sensing in the solar reflective spectrum. In P. S. Thenkabail (Ed.), *Land Resources Monitoring, Modeling, and Mapping with Remote Sensing* (pp. 533–575). Boca Raton, FL, US: CRC Press.

Sun, Y., Frankenberg, C., Jung, M., Joiner, J., Guanter, L., Köhler, P., & Magney, T. (2018). Overview of solar-induced chlorophyll fluorescence (SIF) from the Orbiting Carbon Observatory-2: Retrieval, cross-mission comparison, and global monitoring for GPP. *Remote Sensing of Environment*, *209*, 808–823. https://doi.org/10.1016/j.rse.2018.02.016

Sun, Y., Frankenberg, C., Wood, J. D., Schimel, D., Jung, M., Guanter, L., et al. (2017). OCO-2 advances photosynthesis observation from space via solar-induced chlorophyll fluorescence. *Science*, *358*(6360). https://doi.org/10.1126/science.aam5747

Terrer, C., Vicca, S., Stocker, B. D., Hungate, B. A., Phillips, R. P., Reich, P. B., et al. (2018). Ecosystem responses to elevated CO_2 governed by plant–soil interactions and the cost of nitrogen acquisition. *New Phytologist*, *217*(2), 507–522. https://doi.org/10.1111/nph.14872

Tian, F., Fensholt, R., Verbesselt, J., Grogan, K., Horion, S., & Wang, Y. (2015). Evaluating temporal consistency of long-term global NDVI datasets for trend analysis. *Remote Sensing of Environment*, *163*, 326–340. https://doi.org/10.1016/j.rse.2015.03.031

Tollefson, J. (2015). The 2 °C dream. *Nature*, *521*.

Tramontana, G., Jung, M., Schwalm, C.R., Ichii, K., Camps-Valls, G., Ráduly, B., et al. (2016). Predicting carbon dioxide and energy fluxes across global FLUXNET sites with regression algorithms.

Trenberth, K. E. (2015). Has there been a hiatus? *Science*, *349*(6249), 691–692. https://doi.org/10.1126/science.aac9225

Viovy, N. (2018). CRUNCEP Version 7—Atmospheric Forcing Data for the Community Land Model. In *Research Data Archive at the National Center for Atmospheric Research*. Boulder, CO: Computational and Information Systems Laboratory. https://rda.ucar.edu/datasets/ds314.3/

Wang, D., Morton, D., Masek, J., Wu, A., Nagol, J., Xiong, X., et al. (2012). Impact of sensor degradation on the MODIS NDVI time series. *Remote Sensing of Environment*, *119*, 55–61. https://doi.org/10.1016/j.rse.2011.12.001

Wang, H., Prentice, I. C., Keenan, T. F., Davis, T. W., Wright, I. J., Cornwell, W. K., et al. (2017). Towards a universal model for carbon dioxide uptake by plants. *Nature Plants*, *3*(9), 734–741. https://doi.org/10.1038/s41477-017-0006-8

Welp, L. R., Keeling, R. F., Meijer, H. A., Bollenbacher, A. F., Piper, S. C., Yoshimura, K., et al. (2011). Interannual variability in the oxygen isotopes of atmospheric CO2 driven by El Niño. *Nature*, *477*(7366), 579–582. https://doi.org/10.1038/nature10421

Wolf, J., West, T. O., Le Page, Y., Page Kyle, G., Xuesong, Z., James Collatz, G., & Imhoff, M. L. (2015). Biogenic carbon fluxes from global agricultural production and consumption. *Global Biogeochemical Cycles*, *29*, 1617–1639. https://doi.org/10.1002/2015GB005119

Yuan, W., Cai, W., Xia, J., Chen, J., Liu, S., Dong, W., et al. (2014). Global comparison of light use efficiency models for simulating terrestrial vegetation gross primary production based on the LaThuile database. *Agricultural and Forest Meteorology*, *192*, 108–120.

Zhang, Y., Song, C., Band, L. E., Sun, G., & Li, J. (2017). Reanalysis of global terrestrial vegetation trends from MODIS products: Browning or greening? *Remote Sensing of Environment*, *191*, 145–155. https://doi.org/10.1016/j.rse.2016.12.018

Zhang, Y., Song, C., Sun, G., Band, L. E., McNulty, S., Noormets, A., et al. (2016). Development of a coupled carbon and water model for estimating global gross primary productivity and evapotranspiration based on eddy flux and remote sensing data. *Agricultural and Forest Meteorology*, *223*, 116–131. https://doi.org/10.1016/j.agrformet.2016.04.003

Zhang, Y., Song, C., Sun, G., Band, L. E., Noormets, A., & Zhang, Q. (2015). Understanding moisture stress on light use efficiency across terrestrial ecosystems based on global flux and remote-sensing data. *Journal of Geophysical Research: Biogeosciences*, *120*, 2053–2066. https://doi.org/10.1002/2015JG003023

Zhang, Y., Song, C., Zhang, K., Cheng, X., Band, L. E., & Zhang, Q. (2014). Effects of land use/land cover and climate changes on terrestrial net primary productivity in the Yangtze River Basin, China, from 2001 to 2010. *Journal of Geophysical Research: Biogeosciences*, *119*, 1092–1109. https://doi.org/10.1002/2014JG002616

Zhang, Y., Xiao, X., Wu, X., Zhou, S., Zhang, G., Qin, Y., & Dong, J. (2017). A global moderate resolution dataset of gross primary production of vegetation for 2000–2016. *Scientific data*, *4*(1), 170165. https://doi.org/10.1038/sdata.2017.165

Zhao, M., & Running, S. W. (2010). Drought-induced reduction in global terrestrial net primary production from 2000 through 2009. *Science*, *329*(5994), 940–943. https://doi.org/10.1126/science.1192666

Zhu, Z., Bi, J., Pan, Y., Ganguly, S., Anav, A., Xu, L., et al. (2013). Global data sets of vegetation leaf area index (LAI) 3g and fraction of photosynthetically active radiation (FPAR) 3g derived from Global Inventory Modeling and Mapping Studies (GIMMS) Normalized Difference Vegetation Index (NDVI3g) for the period 1981 to 2011. *Remote Sensing*, *5*, 927–948.

Zhu, Z., Piao, S., Myneni, R. B., Huang, M., Zeng, Z., Canadell, J. G., et al. (2016). Greening of the Earth and its drivers. *Nature Climate Change*, *6*(8), 791–795. https://doi.org/10.1038/nclimate3004